

Engineering Design of a Special Purpose Functional Magnetic Resonance Scanner Magnet

Alice Borceto¹, Daniele Damiani², Andrea Viale¹, Franco Bertora¹, *Member, IEEE*, and Roberto Marabotto²

Abstract—A 2 T open MRI scanner for fMRI investigations of subjects maintaining a natural stance and free access to the environment is presented. The self-shielded multi-coil magnet is composed from solenoids optimized in positions and cross-sectional shape. It provides a room temperature gap of 800 mm at the subject shoulders, tapering down to 600 mm at its narrowest point. The system consists of symmetrical magnetic poles, five NbTi superconducting coils each, maintained at 4.2 K in a liquid helium cryostat with a re-condenser. Windings, coil formers, mechanical structure, cryostat, vacuum chamber, thermal shield, mechanical supports, and cryogenics have been modeled in detail using Catia CAD software, accounting for the interactions among components and the constraints posed by winding and assembly methods. The cable characteristics have been chosen based on simulations of thermodynamic stability in operating conditions; self-protection against quench has been provided by inductance subdivision with bypass diodes.

Index Terms—Field homogeneity, magnetic resonance imaging, magnets, MRI

I. INTRODUCTION

MAGNETIC Resonance Imaging (MRI) is today a well established diagnostic modality and the superconducting MRI magnet industry has reached a state of maturity, with an installed base in excess of 30,000 units and a production rate of the order of 10% of the installed base, to cater for new sites and replacements. [1]. The dominant magnet type is the superconducting solenoid with a field intensity of 1.5 to 3 T, a length of about 1.5 m and an inner bore diameter of 1 m, that translates to a patient bore diameter of about 60 cm. This configuration is not ideal but the limitations it poses do not compromise the balance achieved between scanner cost and clinical usefulness for the majority of the population. The needs of the excluded cases (obese or claustrophobic patients, need of minor interventional medical procedures, etc.) are addressed by the so called open systems, generally characterized by a lower field of about 1 T and a higher cost.

This panorama would satisfy all major needs were it not for the advent of functional MRI (fMRI), a technique allowing to map neural tissue activation consequent to specific tasks that had a strong impact on research. Functional MRI and more recent techniques, such as diffusion tensor imaging (DTI) and diffusion tractography have allowed scientists to make great strides in understanding how the brain functions, and are now the prominent tools in the cognitive neuroscience field. The

technique developed in the early 90s, partly as a consequence of the availability of the (by then) high-field systems at 1.5 T. In fact fMRI relies on three-dimensional volume acquisitions at rates of one volume every 1 or 2 seconds and — because of signal to noise issues — this is possible, with sufficient image quality, only at that field level. Since then the technique has migrated from a pure investigatory mean to the clinical practice and is routinely used today in the planning of surgical brain tumor excisions.

In the cognitive neuroscience research field the technique has been extremely fruitful but has been hampered by the physical constraints imposed by the magnet, that forces the subject to lie in a horizontal position and severely limits his/her capability to interact with the surroundings. This may not represent a limit in the case of cognitive studies but is a serious hindrance when the planning and execution of movements is concerned.

This work describes the engineering design of the magnet for a special purpose scanner to be mainly devoted to the study of the brain motor cortex. The main requirements are a minimum field intensity of 2 T, internal cavity capable to accommodate a human subject in a standing or sitting pose, with enough room to enable the execution of upper limb movements, like those done in ordinary life, while sitting at a table or driving.

II. PREVIOUS WORK

Some comparable attempts have been made in the past, although with different purposes: some of them specifically oriented to intraoperative MRI applications [2] [3] [4] [5] [6] [7] [8] [9] and only one conceived with a similar goal, although apparently limited to the top portion of the brain, with the exclusion of the cerebellum, of the encephalic trunk and of the spine, where significant activity related to the motor system may be found [10] [11] [12] [13].

III. METHODOLOGY

The main magnet has been designed by a multi-coil approach, based on the optimization of several key parameters, such as central field homogeneity, flux leakage, maximum current density, pole diameter and gap size as well as conductor length. Multi-coil design is a standard technique for the design of cylindrical magnets [14], however it can be adopted also for the design of open scanners. In such configurations the main design trade-offs among the significant magnetic challenges are gap size vs. pole diameter, uniformity and stray field

¹A. Borceto, A. Viale and F. Bertora, are with the Robotics, Brain and Cognitive Sciences Dept. of Istituto Italiano di Tecnologia, 16163 Genova, Italy; (e-mail alice.borceto@iit.it)

²D. Damiani and R. Marabotto are with ASG Superconductors S.p.A., 16152 Genova, Italy (e-mail damiani.daniele@as-g.it)

In a multi-coil approach the magnet is composed by a set of solenoids, whose positions are optimized such that the magnet generates the desired homogeneous magnetic fields

The field produced by a system of coils can be expressed in terms of spherical harmonics in any current-free region. In particular, the field produced by coaxial circular coils on a sphere centered on their axis (z) and not enclosing any coil, can be expressed in terms of zonal harmonics only [15], as:

$$\vec{B}_{in} = \sum_{n=0}^{\infty} d_n r^n P_n(\cos\theta) \vec{e}_z$$

where:

\vec{e}_z is the unit vectors along the z axis,
 $P_n \cos(\theta)$ are the Legendre functions.
 r and θ represent the spherical coordinates of the test point,
 and d_n the multipole field coefficients corresponding to the strengths of the harmonics.

Similarly the field outside a sphere completely enclosing the coil can be written as

$$\vec{B}_{out} = \sum_{n=1}^{\infty} \frac{c_n}{r^{n+2}} P_{n+1}(\cos\theta) \vec{e}_z$$

where c_n are the multipole field coefficients. Expressions for the computation of c_n and d_n in the case of rectangular cross-section circular coils can be found in [14].

The feasible coil space is densely sampled by a matrix of candidate solenoids and the coefficient $c_{n,i}$ and $d_{n,i}$ computed for each harmonic order n and unit current density in each solenoid i . Current densities j_i are taken as unknowns and are optimized by linear programming (LP) such that the magnitude of the expansion coefficient of the central field does not exceed the given design values D_{n_1}, D_{n_2}, \dots , where n_1, n_2, \dots are the orders of the harmonics.

The optimization procedure can be formulated as:

$$\begin{aligned} & \min_{l_i, j_i} \sum_i l_i |j_i| \\ & \text{subject to} \\ & D_n - tol_n \leq \sum_i d_n j_i \leq D_n + tol_n \\ & |j_i| \leq j_{max} \end{aligned} \quad (1)$$

For shielded magnet configuration constraints can be similarly imposed on the harmonics in the outer sphere

$$C_m - tol_m \leq \sum_i c_i j_i \leq C_m + tol_m \quad (2)$$

where $tol_{n,m}$ are the tolerances of the inner and outer error field on the z -axis, and l_i is the mean circumferential length of the i^{th} solenoid. The presence of l_i in the objective function, allows to optimize conductor length and hence to decrease the magnet cost.

By changing the optimization variables such as maximum current density, and the area of the feasible space, different geometries with different gap size and pole diameter have been evaluated. Since increasing the gap makes the whole

TABLE I
 CONDUCTOR CHARACTERISTICS

Bare conductor dimensions	3.88 × 2.59 mm
Insulated conductor dimension	4.13 × 2.84 mm
Insulation	Fiberglass
Critical current	3350 A @ 4.2 K, 5 T
Superconducting area	1.62 mm ²
Copper area	8.43 mm ²
Copper/Superconductor ratio	5.2
Packing Factor	85.3%
Number of filament	84
Twist pitch	100 mm

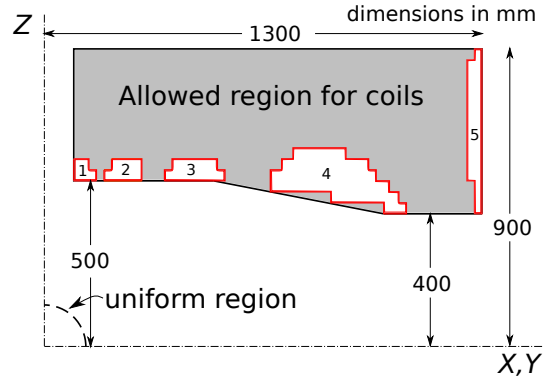


Fig. 1. Allowed regions and resulting coil cross-sections (only a quarter of the structure is shown).

design very challenging in terms of conductor length and pole diameter, a stepped gap configuration has been devised, that leaves to the subject an elbow to elbow space of 80 cm and unimpaired frontal visibility although the access is restricted to 60 cm. Such dimensions not only offer the possibility to sit or to stand, but also allow reasonably free limb movements and a direct perception of the surrounding environment. The counterpart is a pole radius that has to be of the order of 1.5 m, increasing somewhat the conductor length.

IV. RESULTS

Conductor choice

The conductor, whose characteristics are shown in Table I, consists of multifilamentar NbTi wire with a copper matrix for stabilization, insulated, with rectangular cross section.

The design has been carried over on the basis of the initial conductor choice and of the basic design parameters:

field intensity	harmonic coeff $D_0 = 2$ [T]
homogeneity	null harmonic coeffs D_n up to 8 th order included, on .25 m dia sphere
stray field	null harmonic coeffs C_m up to 4 th order included, on 4 m dia sphere
tolerance	$tol_n = tol_m = 10$ ppm.
allowed coil region	as show in Fig. 1

The solution to (1) and (2) obtained by linear programming satisfies a maximum sparsity property and naturally concentrates the current density in contiguous areas where it is set to the maximum available value, with the exception of the border cells where it assumes a different value.

To simplify the manufacturing these boundary cells have been given the same current density as the adjacent ones but their area has been proportionally reduced in order to disturb minimally the solution. The resulting coil profile are indicated by the heavy contours in Fig. 1. The overall current density in the coils is 90 A/mm² and alternates in sign from the center to the periphery.

Thermodynamic stability and protection verification

The magnetic field intensity at the conductor locations has been computed by means of a finite elements code (Opera by Cobham Associates) which assessed a maximum field intensity of 7.25 T at the internal periphery of coil #4, as shown in Fig. 2. The nominal current is 1056 A, with a current density of 105 A/mm² on the bare conductor. This information is necessary to verify the magnet thermal stability and to define its protection. The first criterion seeks a low quench probability while the second ensures that in case of quench the magnet is not damaged.

First of all, the thermal and electrical characteristics of an equivalent cell, composed of the bare conductor (copper and superconductor), and of its shell composed of fiber glass tape impregnated with epoxy resin, have been computed on the basis of the geometry and of the physical parameters of the constituent parts.

The thermodynamic stability has been verified solving the thermal equation by finite differences considering a one-dimensional superconductor having the electrical and thermal characteristics determined for the equivalent cell in a stationary and adiabatic regime. This can be considered a worst case situation since it neglects the thermal exchanges that take place with the neighbouring turns in a real winding. At the determined maximum field intensity on the conductor of 7.25 T, the minimum propagating zone (MPZ) and the minimum quench energy (MQE) have been determined numerically resulting in MPZ and MQE values of 34 mm and 1.2 mJ. The temperature margin results to be 0.76 K, an acceptable value for liquid Helium cooling, and a MQE of 1.2 mJ over 34 mm gives a specific energy of about 3000 J/m³; about an order of magnitude lower than what can be delivered by a crack in the resin [16]. Given these results some training could be expected but it is necessary to remember that the initial premises were a worst case.

The protection of the magnet by means of an external dump resistor turns out to be unfeasible, given the high voltage that would be reached if the max temperature of the hot spot must be kept below 150 K, so a different strategy has to be considered. The high quench propagation velocity, which results to be 7.5 m/s, suggests to employ the coils themselves to dissipate the magnet energy; however, given that the inductance is rather high, it will be necessary to section some of the coils before employing cold bypass diodes. Considering the inner layers of the most stressed coil (#4) it can be seen that a diode with a threshold voltage of 0.7 V in parallel with the first 480 turns (self inductance 1.3 H) would start conducting after 45 ms, limiting the maximum temperature at the end of the quench to 86 K and confirming

the feasibility of this form of protection. Quench calculation has been performed with the finite difference code MagZift [17].

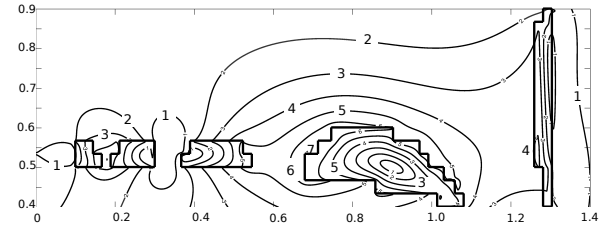


Fig. 2. Magnetic field intensity in the windings area. The maximum field is on the internal surface of coil #4 (only 1/4 of the coils cross-section is shown).

Coil Formers and Windings

The five coils will have to be wound on suitable formers, as those shown in Fig. 3 that will also serve the purpose of receiving and distributing the axial electromechanical forces that reach up to 9 MN and the radial stresses. Once wound each coil and the relative forming block are vacuum impregnated with resin and form a monolithic block.

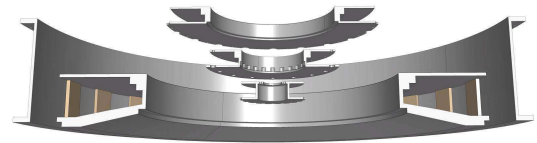


Fig. 3. The five winding forms. Forms 1,4 and 5 are in their final position while forms 2 and 3 have been moved up for clarity.

The cross-section of the coils resulting from the optimization is unusual. However, their reduction to a conventional rectangular cross section, while preserving the design requirements, would have sensibly increased the conductor length limited to 75.8 km, with an Amp×Length value of 80, somewhat above the range of a typical cylindrical 3 T magnet [1]. It has to be remembered that we are dealing here with a very open and therefore inefficient configuration

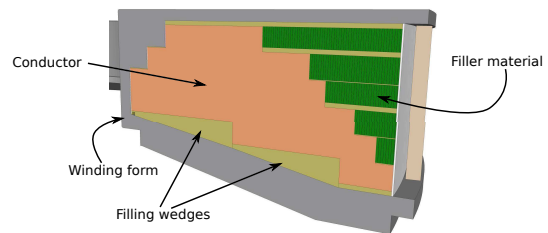


Fig. 4. The shape of coil #4 requires special cares in the winding to ensure a smooth transition from every layer to the next.

While coils 1,2,3 and 5 do not pose excessive winding problems, coil #4 presents only one side that does not have a staircase profile (see Fig. 4) and requires special care to ensure that all layers reach exactly the same diameter of the pre-inserted filling wedge, to ensure a smooth basis for the subsequent layer. This requires a constant attention and the

application of suitable corrections in the form of modulation of conductor tension, and/or insertion of shims during the winding process.

Mechanical Structure

The mechanical structure must sustain the coil weights and the electromechanical forces acting on them, that are more significant coil #4 is pulled axially towards its symmetrical with a force of about 9 MN and the couple of coils #5 repel with a force of about 6.2 MN the net resultant being a 2.7 MN attracting force between the two poles. These forces are coped with by two massive disks and the whole structure is supported on four feet, as shown in Fig. 5.

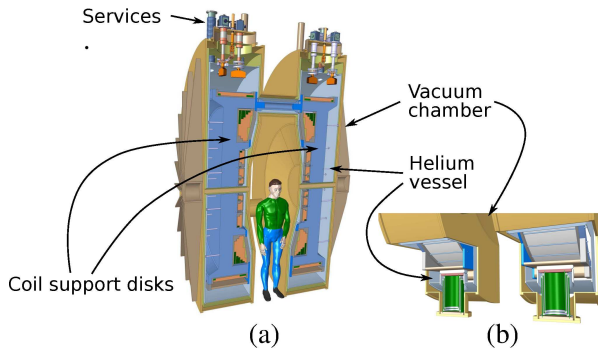


Fig. 5. a) The mechanical structure consists of two massive disks that support the coils and are kept together by three pillars. b) Detail of the four composite support feet that ensure the thermal insulation of the cold mass.

Vacuum and Helium Chambers

The system cooling is ensured by a liquid Helium bath in a vessel at a pressure slightly superior to atmospheric pressure. The Helium is continually recondensed by cryocoolers located in the upper part of the chamber, where it recollects. The vessel is designed for the maximum overpressure that can arise in case of quench. A thermal screen is located between the cold mass and the vacuum chamber that surrounds; it is thermally anchored at an intermediate point of the cryocoolers at the top of the system and at an intermediate point of the thermal path of the feet.

The four feet that support the magnet have a telescoping composite structure made up of impregnated fiber glass and stainless steel sections arranged so that the fiber glass is subjected to compression and the steel to traction.

The vacuum chamber is split in two parts, one for each pole, connected through tubes concentric to the pole pillars. The top portion hosts the cryogenic, electrical, hydraulic and control services for the system.

V. DISCUSSION

The main purpose of this work was to establish the feasibility of a high-field wide-gap open MRI magnet to investigate areas of the motor cortex or of the brain stem during the execution of motor tasks. The initial goal of a field intensity of 2 T over a 25 cm diameter of spherical volume (DSV) was

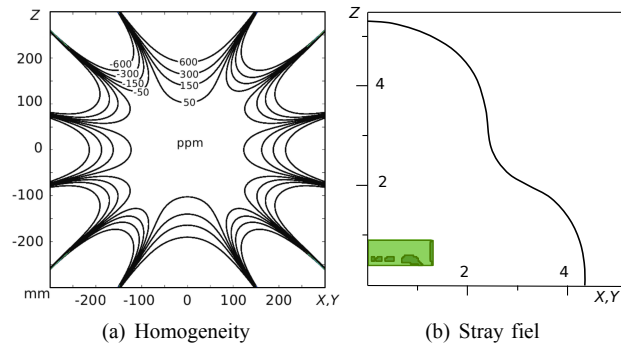


Fig. 6. a) Field homogeneity in ppm, b) 5 G stray field line (scale in meters)

TABLE II
MAGNET CHARACTERISTICS

Room temperature gap	60-80 cm
Field at center	2 T
Field uniformity before shimming	156 ppm over 25 cm DSV
Stray field (5 G line)	5.3×4.3 m
Stored energy	31.7 MJ
Inductance	57 H
Conductor length	75.8 km
Current density	90 A/mm ²
Dimensions	4×3.8×4.6 m (DWH)
Weight	60 ton

chosen as a compromise between overall cost and suitability for the purpose and a complete magnetic design has been carried over. The magnetic design has been then turned into an engineering design the final outcomes of which do not represent yet the blueprints for an actual construction but are close enough to it, in order to clearly state its feasibility and the budgetary cost of the implementation.

The final design has the characteristics shown in detail in Table II; the uniform field region is a slightly flattened sphere of sufficient extent (see Fig. 6 that also shows the stray field) the elbow to elbow room for the subject is 80 cm, enough to carry on most desktop tasks with natural ease.

The subject field of view (not considering any restriction due to the imaging coils) is virtually unlimited in the vertical direction while horizontally it spans 72 degrees, gradually decreasing to 30 at distances ranging from 50 cm to 1 m from the center of the head, and finally limited to 20 degrees at infinity. By everyday standards this may be considered restricted but can be easily augmented using current virtual reality technology.

As it could have been expected the amount of conductor employed is larger than that necessary for a conventional cylindrical magnet. This is the price to pay for openness that anyway poses this design halfway between today's 3 T and 7 T standards, with a stray field imprint that is close to that of a 3 T. All these figures could be made better at the cost, however, of a steep increase in costs that is probably not justifiable for such a special purpose.

REFERENCES

- [1] T. C. Cosmos and M. Parizh, "Advances in whole-body MRI magnets," *IEEE Transactions on Applied Superconductivity*, vol. 21, no. 3, pp. 2104-2109, June 2011.

- [2] Y. Lvovsky and P. Jarvis, "Superconducting systems for MRI; present solutions and new trends," *IEEE Transactions on Applied Superconductivity*, vol. 15, no. 2, p. 1317, 2005.
- [3] B. Baodong, Z. Yanli, X. Dexin, and X. Pingchou, "Study on a fully open magnetic resonance imaging device with a slice imaging region," in *Proceedings of the 2005 IEEE Engineering in Medicine and Biology 27th Annual Conference Shanghai, China, September 1-4, 2005*, pp. 7008–7011.
- [4] Y. Yao, Y. Fang, C. S. Koh, and G. Ni, "A new design method for completely open architecture permanent magnet for MRI," *IEEE Transactions on Magnetics*, vol. 41, no. 5, p. 1504, 2005.
- [5] Y. Yao, Y. Fang, G. Ni, and C. S. Koh, "The optimal design method of completely open architecture permanent magnet for magnetic resonance imaging," in *Progress In Electromagnetics Research Symposium 2005*, 2005, pp. 23–26.
- [6] C. Nimsky, R. Fahlbusch, O. Ganslandt, and B. Keller, "Intraoperative bildgebung mit 1,5-tesla-hochfeld-magnetresonanztomographie," *Journal für Neurologie, Neurochirurgie und Psychiatrie*, vol. 6, pp. 34–43, 2005.
- [7] C. Nimsky, A. Fujita, O. Ganslandt, B. von Keller, E. Kohmura, and R. Fahlbusch, "Frameless stereotactic surgery using intraoperative high-field magnetic resonance imaging," *Neurol Med Chir (Tokyo)*, vol. 44, pp. 522–534, 2004.
- [8] F. Jolesz, "Future perspectives for intraoperative MRI," *Neurosurgery Clinics of North America*, vol. 16, no. 1, p. 201, 2005.
- [9] G. R. Sutherland and D. F. Louw, "Intraoperative MRI: a moving magnet," *CMAJ*, vol. 161, no. 10, p. 1293, 1999.
- [10] T. Nakada and N. Tasaka, "Human brain imaging in the upright position," *Neurology*, vol. 57, pp. 1720–1722, 2001.
- [11] H. Kitaguchi, O. Ozaki, T. Miyazaki, N. Ayai, K. Sato, S. Urayama, and H. Fukuyama, "Development of a Bi-2223 HTS magnet for 3 T MRI system for human brains," *IEEE Transactions on Applied Superconductivity*, vol. 20 n. 3, pp. 710–713, 2010.
- [12] S. Urayama, O. Ozaki, H. Kitaguchi, I. Nakajima, N. Ohnishi, M. Poole, K. Sato, and H. Fukuyama, "Cryogen-free 3 T-MRI system for human brain research using Bi-2223 high-temperature superconducting tapes," in *Proceedings of 2012 ICME International Conference on Complex Medical Engineering*, 2012.
- [13] T. Nakada, "Clinical experience on 3.0 T systems in Niigata, 1996 to 2002," *Invest. Radiol.*, vol. 38, pp. 377–384, 2003.
- [14] M. Kitamura, S. Kakugawa, and K. Maki, "An optimal design of coaxial coils with constraints on inner and outer multipole magnetic field," *IEEE Transactions on Applied Superconductivity*, vol. 14, pp. 1862–1866, June 2004.
- [15] F. Roméo and D. I. Hoult, "Magnet field profiling Analysis and correcting coil design," *Magnetic Resonance in Medicine*, vol. 1, no. 1, pp. 44–65, 1984. [Online]. Available: <http://dx.doi.org/10.1002/mrm.1910010107>
- [16] M. N. Wilson, *Superconducting Magnets*. Oxford University Press, 1987.
- [17] Y. Eyssa and W. Markiewicz, "Quench simulation and thermal diffusion in epoxy-impregnated magnet system," *IEEE Transactions on Applied Superconductivity*, vol. 5, no. 2, pp. 487–490, 1995.